

FRIH: Fine-grained Region-aware Image Harmonization

Jinlong Peng¹, Zekun Luo¹, Liang Liu¹, Boshen Zhang¹, Tao Wang²,
Yabiao Wang¹, Ying Tai¹, Chengjie Wang¹, Weiyao Lin²

¹Tencent Youtu Lab

²Shanghai Jiao Tong University

{jeromepeng,zekunluo,leoneliu,boshenzhang,caseywang,yingtai,jasoncjwang}@tencent.com
{wang_tao1111,wylin}@sjtu.edu.cn

ABSTRACT

Image harmonization aims to generate a more realistic appearance of foreground and background for a composite image. Existing methods perform the same harmonization process for the whole foreground. However, the implanted foreground always contains different appearance patterns. All the existing solutions ignore the difference of each color block and losing some specific details. Therefore, we propose a novel global-local two stages framework for Fine-grained Region-aware Image Harmonization (FRIH), which is trained end-to-end. In the first stage, the whole input foreground mask is used to make a global coarse-grained harmonization. In the second stage, we adaptively cluster the input foreground mask into several submasks by the corresponding pixel RGB values in the composite image. Each submask and the coarsely adjusted image are concatenated respectively and fed into a lightweight cascaded module, adjusting the global harmonization performance according to the region-aware local feature. Moreover, we further designed a fusion prediction module by fusing features from all the cascaded decoder layers together to generate the final result, which could utilize the different degrees of harmonization results comprehensively. Without bells and whistles, our FRIH algorithm achieves the best performance on iHarmony4 dataset (PSNR is 38.19 dB) with a lightweight model. The parameters for our model are only 11.98 M, far below the existing methods.

1 INTRODUCTION

Image composition plays an essential role in image editing and generation [1, 5, 11, 12, 20, 26, 34, 36]. However, since the source of the implanted foreground object and the new background image are different, it is easy to cause an unrealistic perception of the composite image. Image harmonization is an important operation to address this issue, which aims to make the implanted foreground compatible with the background.

Traditional image harmonization methods mainly focused on low-level feature statistics, such as color distribution matching [6, 24, 25], gradient-domain compositing [16, 23, 32] and hybrid feature transferring [31]. These methods limit the harmonization performance due to the lack of high level information. There are also several unsupervised or self-supervised image harmonization methods [3, 17, 39], which does not rely on manual annotation. But they only work better in specific scenes, such as the portraits harmonization, lack of universality. Recently, the supervised encoder-decoder harmonization methods [8, 14, 19, 33] have achieved superior performance based on the construction of the large training datasets.

However, there is still a major problem of existing solutions. The implanted foreground always contains different appearance

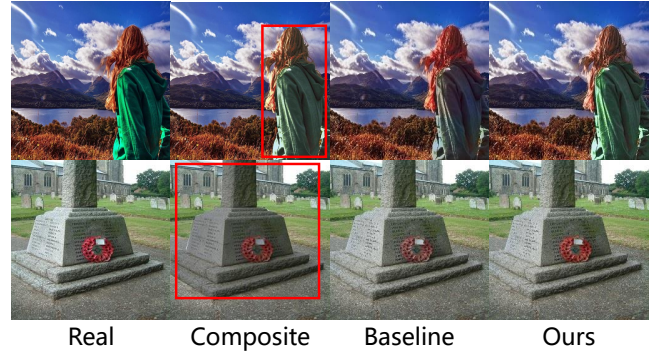


Figure 1: Case study on the coarse-grained harmonization problem of different foreground appearance patterns. On the top line, the implanted foreground is a person with green shirt and orange hair. The background contains more orange pixels, leading to a better harmony of the orange hair, while the green saturation in the clothes decreases in baseline. On the bottom line, the implanted foreground is a gray sculpture and a red wreath. The background is brighter, resulting in a brighter overall harmony process in baseline. The gray sculpture looks good while the red wreath becomes too whiter. Clearly, our fine-grained region-aware image harmonization algorithm could solve the above problem well.

patterns. The similarity between the composite image and the real ground-truth image varies among different sub-regions. Some sub-regions in the composite image are relatively similar to the real ground-truth image, while others may be much far away from the target. Thus different sub-regions need different harmonization operations. Existing methods perform the same harmonization process for the whole foreground, ignoring the difference of each color block and losing some specific details. As can be seen in Figure 1, the foreground of the first case is a person with green shirt and orange hair. The foreground of the second case is a gray sculpture and a red wreath. If applying the coarse-grained harmony process (baseline), only part of the foreground (the orange hair and the gray sculpture) has satisfactory harmonization performance, while the other part (the green shirt and the red wreath) is ineffective.

In order to solve the above problem, we propose a simple, novel and effective global-local framework for Fine-grained Region-aware Image Harmonization (FRIH), which is a two-stage network. The first stage includes the base network (a simple U-Net [28] alike

network), in which the composite image and the whole input foreground mask is used to make a global coarse-grained harmonization. In the second stage, we adjust the global harmonization performance according to the region-aware local feature. Specifically, we adaptively cluster the input foreground mask into several submasks by the corresponding pixel RGB values in the composite image. The number of the submasks is adaptive for different input images. Each submask and the coarsely adjusted image are concatenated respectively and fed into a lightweight cascaded module. Moreover, in order to utilize the different levels of the harmonization results comprehensively, we further designed a fusion prediction module by fusing features from all the cascaded decoder layers together to generate the final result. Note that our two-stage network FRIH is trained end-to-end. If the two stages are trained separately, the submasks information can not affect the training of the first stage, not able to maximize the optimization of the overall performance.

Our FRIH method achieves the best performance in iHarmony4 [8] dataset with a lightweight model. The PSNR of our method is 38.19 dB, performing better than all the existing SOTA methods [8, 14, 19]. Specifically, the sub-regions details of the two cases in Figure 1 are both handled well by our method. Besides, our model has only 11.98 M parameters, which is only 1/5 of the existing SOTA methods [8, 14, 19]. The base network has 9.30 M parameters and the lightweight cascaded module together with the embedded fusion prediction module has 2.68 M parameters, only accounting for 22.4% of the parameters of the whole FRIH network. The main contributions of this paper are listed as follows:

1. We propose a simple, novel and effective global-local framework for fine-grained region-aware image harmonization (the first as far as we know). The local submasks are generated adaptively to adjust the global coarse-grained harmonization.

2. We design a lightweight cascaded module to integrate the global coarsely adjusted image and the region-aware local feature, refining the harmonization performance. And the fusion prediction module is further proposed to utilize the different degrees of harmonization results comprehensively.

3. Our FRIH achieves the best PSNR (38.19) on iHarmony4 dataset. Besides, the parameters of our model are only 11.98 M, which is far lower than existing methods.

2 RELATED WORKS

2.1 Statistics-based Harmonization Methods

Traditional image harmonization methods mainly focused on low-level feature statistics, such as color distribution matching [6, 24, 25, 30], gradient-domain compositing [16, 23, 32] and hybrid feature transferring [31]. These methods did not consider the realism of the composite images. Several other methods [18, 38, 40] further applied high-level image feature to design the visual reality assessment mechanism. Despite the better optimization standards, the basis of these methods is still statistics methods, limiting the harmonization performance. While our FRIH follows the currently mainstream supervised encoder-decoder framework, which has the potential for better harmonization results.

2.2 Encoder-decoder Harmonization Methods

Comparing with traditional statistics-based methods, recent encoder-decoder harmonization methods have achieved superior performance. The pioneering end-to-end CNN method DIH [33] encoded the input image and foreground mask, which was then decoded to the harmonized image and scene parsing image. Based on the encoder-decoder framework, several methods [7–9, 15] applied the attention mechanism to learn foreground and background appearance feature separately for harmonization. Moreover, RainNet [19] designed a region-aware adaptive instance normalization module to transfer the visual style from background to foreground. IHH [14] proposed intrinsic image harmonization framework by disentangling the composite image into reflectance and illumination for further separate harmonization. Guo *et. al* [13] integrated the transformer structure [10, 35] to the encoder-decoder harmonization network. However, all these methods only divided the foreground and background as different regions. They did not make a finer region division inside the foreground. Differently, our FRIH is the first method to propose the fine-grained region-aware harmonization framework, which could get more precise harmonization results.

2.3 Cascade Mechanism

Cascade mechanism is a direct but useful strategy in many computer vision tasks [2, 4, 22]. The key idea is to use an extra cascaded module to refine the results from the previous stages. In object detection task, Cascade R-CNN [2] used a sequence of detectors trained with increasing IoU thresholds to gradually refine the detection results from the previous detectors. CU-Net [21] connected two U-Net networks and used two stage loss supervision for more accurate segmentation. Cascade EF-GAN[37] decomposed the expression editing task into three steps and applied three cascaded GANs to solve each of them. Most of these methods used the same architecture of base network to design their cascaded module, leading to a large increase of model size. Different from those methods, our cascaded module is lightweight and effective. The lightweight module together with the embedded fusion prediction module only accounts for 22.4% of the parameters of the whole FRIH network.

3 PROPOSED METHOD

3.1 Overview

The definition of image harmonization is to input a composite image with the corresponding foreground mask and output the harmonious image. Formulaically, the composite image I_c consists of the foreground image I_f and the background image I_b . The foreground mask M_f denotes the foreground region in the composite image I_c . The background mask $M_b = 1 - M_f$ accordingly. The goal of image harmonization network is training a generator G to generate the harmonious image \hat{I} , where $\hat{I} = G(I_c, M_f)$. If there is a ground-truth image I of the composite image I_c , the optimization direction of the model G is to make \hat{I} close to I .

Our proposed fine-grained region-aware image harmonization framework is illustrated in Figure 2, which is a two-stage network. We use a simple U-Net [28] alike network as the base network in the first stage. In this stage, we feed the composite image and the foreground mask into the encoder-decoder network to obtain the

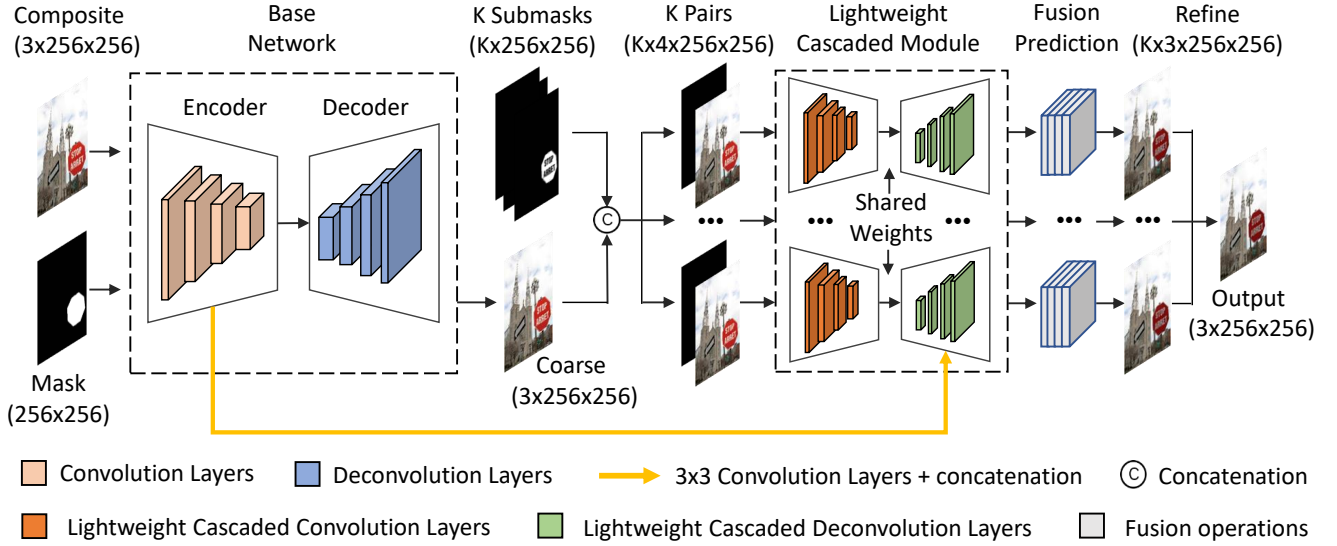


Figure 2: Our proposed FRIH framework. In the first stage, we feed the composite image and the foreground mask into the base network to obtain the coarsely adjusted image. In the second stage, the coarsely adjusted image and the extracted submasks are concatenated respectively and fed into the lightweight cascaded module together with the embedded fusion prediction module, which adjusts the sub-regions and generates final refined harmonious images. Note that to keep the figure clean, we omit the skip connections between the encoder and the decoder, both in the base network and the lightweight cascaded module.

global coarsely adjusted image. In the second stage, we first cluster the foreground mask into several submasks adaptively. Then, each submask and the global coarsely adjusted image generated in the first stage are concatenated respectively and fed into the lightweight cascaded module, which makes full use of the region-aware local feature according to the submasks. Finally, we embeds the fusion prediction module into the decoder of the lightweight cascaded module, to utilize the different levels of the harmonization results comprehensively and generate the final refined harmonious images. The whole FRIH network is trained end-to-end.

3.2 Base Network

The base network inputs the composite image and the foreground mask, and outputs the global coarsely adjusted image. The base network is a simple U-Net [28] alike network, including an encoder and a decoder. The encoder has been downsampled for 7 times and the decoder has 7 deconvolution layers correspondingly. There is a skip connection between each convolution layer in the encoder and the corresponding deconvolution layer with the same feature map size in the decoder.

3.3 Submask Extraction

A significant step of FRIH is to extract the submasks of the global mask. The number K of the submasks needs to be adaptive for different input images. Therefore, We apply CFSFDP clustering algorithm [27] to extract K submasks for each global mask. The original CFSFDP algorithm has two basic ideas, which are that cluster centers have a higher density than their neighbors, and are

at a relatively large distance from points with higher densities [27]. In our method, we cluster the pixels by their corresponding pixel RGB values in the composite image. The local density ρ_i of pixel p_i is measured as:

$$\rho_i = \sum_j \chi(d_{ij} - d_c) \tag{1}$$

where d_{ij} is the normalized euclidean distance between the (r, g, b) vectors of pixels p_i and p_j . d_c is the cutoff distance. We will introduce the setting of d_c in Section 4. $\chi(x) = 1$ if $x < 0$ and $\chi(x) = 0$ otherwise. The minimum distance δ_i between pixel p_i and any other pixel p_j with higher density is defined as:

$$\delta_i = \min_{j:\rho_j > \rho_i} (d_{ij}) \tag{2}$$

Note that if p_i has the highest density in the image, then $\delta_i = \max_j (d_{ij})$. In our method, according to the statistical observations on a large number of images, we find that the appropriate number of submasks for the foreground will not exceed 10 in the vast majority of cases. Therefore, we sort all pixels by δ . The 10 RGB values with the highest δ are considered to be the candidate cluster centers. Note that the RGB values of different candidate cluster centers should be different. For example, if all the pixels in the foreground have the same RGB value, there will be only 1 candidate cluster centers. The candidate cluster centers whose densities ρ do not exceed 10 will be considered as isolated outliers. Only the candidate cluster centers whose densities are higher than 10 are considered as the final cluster centers. Thus the cluster centers of each foreground mask are obtained adaptively. The number of the cluster centers K is in the range of 1 to 10.

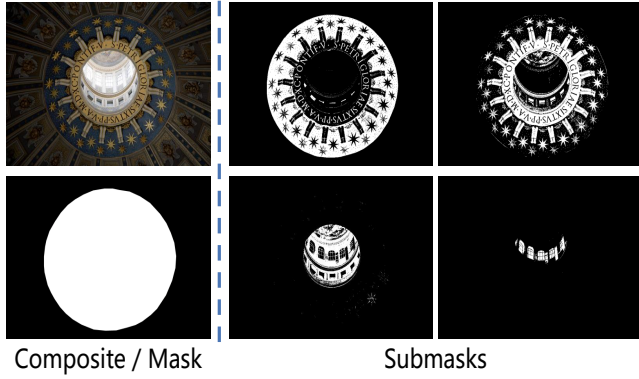


Figure 3: A representative case of the submask extraction. The origin mask (left) is divided into 4 submasks (right).

When all the cluster centers are obtained, the remaining pixels are assigned to the same cluster as their nearest pixel (measured by the normalized euclidean distance of RGB values) of higher density.

In this way, all the pixels in the foreground mask M_f are assigned into K clusters. For each composite image, we obtain K submasks $Subm^1, Subm^2, \dots, Subm^K$. Figure 3 displays a representative set of the generated submasks. In this case, $K = 4$.

3.4 Lightweight Cascaded Module

In this module, we concatenate the global coarsely adjusted image generated in the first stage and each submask respectively. All the concatenated pairs are fed into the lightweight cascaded module. We imitate the structure of U-Net [28] to construct the lightweight cascaded module. In the cascaded encoder, seven 4×4 convolution layers are used to extract different level features of the coarsely adjusted image. In the cascaded decoder part, different from the original decoder in U-Net, at each layer, we use a 1×1 convolution layer to fuse the features from three sources: the previous decoder layer, the corresponding encoder layer in the first stage (the yellow arrow in Figure 2), the corresponding encoder layer in the cascaded module. In this way, we not only further harmonize the image based on the results from first stage network, but also utilize the features from the original composite image. The details of this module are shown in Figure 2. Thus the output of the i -th cascaded decoder layer DC_i can be calculated by the following equation:

$$ET_i = Conv_{trans}(E_i) \tag{3}$$

$$F_i = Conv_{fuse}([DC_{i-1}, ET_i, EC_i]) \tag{4}$$

$$DC_i = Conv_{up}(F_i) \tag{5}$$

where EC_i denotes the output of the i -th layer in the cascaded encoder, which contains the information from the coarsely adjusted image. DC_i denotes the output of the i -th layer in the cascaded decoder. E_i denotes the features from the first stage encoder. We use two 3×3 convolution layers as transfer function $Conv_{trans}$ to transfer this feature E_i into ET_i to make it suitable for the cascaded module. The operator $[]$ means the concatenation operation and

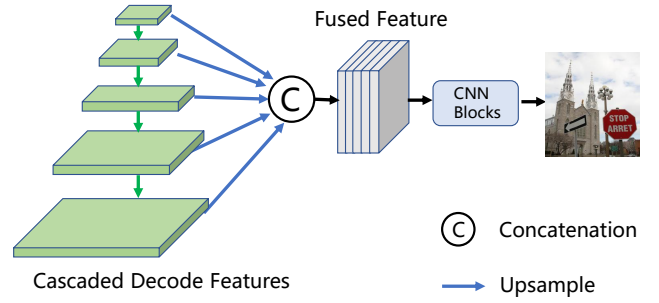


Figure 4: The fusion prediction module. Features from all the cascaded decoder layers are used to predict results.

$Conv_{fuse}$ is a 1×1 convolution layer to fuse the features from three different sources. $Conv_{up}$ is a 4×4 transpose convolution layer to upsample and decode the fused feature F_i . In this way, we obtain the cascaded adjust features from the last layer of our cascaded module. Note that the channels of the features are much smaller than those in the original U-Net. The cascaded module together with the following embedded fusion prediction module has only 2.68 M parameters, only accounting for 22.4% of the parameters of the whole FRIH network. Thus, our cascaded module is lightweight.

3.5 Fusion Prediction

In order to utilize the different levels of harmonization results comprehensively, we further designed the fusion prediction module. In the previous image harmonization methods and traditional U-Net, they only use the features from the last decoder layer to predict the generated images. This is because that the features from the former decoder layers have not been adjust to be close to the target enough. However, in our cascaded module, the input is the coarsely adjusted image. Therefore, all the cascaded decoder layers have already fused the information of the coarsely harmonized image. The outputs from different cascaded decoder layers represent that the features of images that are adjusted to varying degrees. The similarity between the composite image and the real ground-truth image varies among different sub-regions. Some sub-regions in the composite image are relatively similar to the real ground-truth image, while others may be much far away from the target. Thus different sub-regions need different degrees of harmonization. As shown in Figure 4, we fuse features from all the cascaded decoder layers together to predict the harmonized result, which enables the prediction head to utilize features from different harmonization levels. Since the resolution of the features from different cascaded decoder layers are different, we upsample all these feature maps to the resolution 256×256 and concatenate them together. Then we use two 3×3 and one 1×1 convolution layers to convert these fused feature maps to a 3-channel RGB image.

As shown in Figure 2, we can obtain K refined harmonious images from the input K pairs. The final output is generated by combining these images according to the corresponding submasks.

Table 1: Comparison of image harmonization results in each sub-dataset on iHarmony4 test set.

Sub-dataset Metric	HCOCO		HAdobe5k		HFlickr		Hday2night		All	
	MSE↓	PSNR↑								
Input composite	69.37	33.94	345.54	28.16	264.35	28.32	109.65	34.01	172.47	31.63
Lalonde [18]	110.10	31.14	158.90	29.66	329.87	26.43	199.93	29.80	150.53	30.16
Xue [38]	77.04	33.32	274.15	28.79	249.54	28.32	190.51	31.24	155.87	31.40
Zhu [40]	79.82	33.04	414.31	27.26	315.42	27.52	136.71	32.32	204.77	30.72
DIH [33]	51.85	34.69	92.65	32.28	163.38	29.55	82.34	34.62	76.77	33.41
S ² AM [9]	41.07	35.47	63.40	33.77	143.45	30.03	76.61	34.50	59.67	34.35
DoveNet [8]	36.72	35.83	52.32	34.34	133.14	30.21	54.05	35.18	52.36	34.75
ADFM [15]	-	36.87	-	34.99	-	33.36	-	34.31	-	35.86
BargainNet [7]	24.84	37.03	39.94	35.34	97.32	31.34	50.98	35.67	37.82	35.88
IIH [14]	24.92	37.16	43.02	35.20	105.13	31.34	55.53	35.96	38.71	35.90
RainNet [19]	-	37.08	-	36.22	-	31.64	-	34.83	-	36.12
iDIH [29]	19.29	38.44	30.87	36.09	84.10	32.61	55.24	37.26	30.56	37.08
D-HT [13]	16.89	38.76	38.53	36.88	74.51	33.13	53.01	37.10	30.30	37.55
FRIH (ours)	15.05	39.35	23.61	37.69	68.93	33.48	42.78	37.89	23.98	38.19

Table 2: Comparison of image harmonization results in each foreground ratio range on iHarmony4 test set.

Foreground ratios Metric	0%-5%		5%-15%		15%-100%		All	
	MSE↓	fMSE↓	MSE↓	fMSE↓	MSE↓	fMSE↓	MSE↓	fMSE↓
Input composite	28.51	1208.86	119.19	1323.23	577.58	1887.05	172.47	1387.30
Lalonde [18]	41.52	1481.59	120.62	1309.79	444.65	1467.98	150.53	1433.21
Xue [38]	31.24	1325.96	132.12	1459.28	479.53	1555.69	155.87	1411.40
Zhu [40]	33.30	1297.65	145.14	1577.70	682.69	2251.76	204.77	1580.17
DIH [33]	18.92	799.17	64.23	752.86	228.86	768.89	76.77	773.18
S ² AM [9]	15.09	623.11	48.33	540.54	177.62	592.83	59.67	594.67
DoveNet [8]	14.03	591.88	44.90	504.42	152.07	505.82	52.36	549.96
BargainNet [7]	10.55	450.33	32.13	359.49	109.23	353.84	37.82	405.23
RainNet [19]	11.66	550.38	32.05	378.69	117.41	389.80	40.29	469.60
iDIH [29]	8.38	366.32	25.39	287.02	89.44	297.94	30.56	330.45
FRIH (ours)	6.89	305.28	19.88	226.45	70.05	205.83	23.98	252.63

3.6 Training Loss

Since we use base network to predict coarse results and a cascaded module to obtain refined images, for each image, the loss function L_{total} of FRIH consists of two parts, which are L_{coarse} and L_{refine} . we use the following equation to calculate L_{total} .

$$L_{total} = L_{coarse} + L_{refine} \quad (6)$$

$$L_{coarse} = \sum_{h,w} \frac{\|I_{h,w} - \hat{I}_{h,w}\|_2^2}{\max(\text{Area}_{mask}, A_{min})} \quad (7)$$

$$L_{refine} = \sum_{i=1}^K \sum_{h,w} \frac{\|I_{h,w} - \hat{I}_{h,w}\|_2^2 \cdot \text{Subm}_{h,w}^i}{\max(\text{Area}_{\text{Subm}^i}, A_{min})} \quad (8)$$

where \hat{I} is the prediction result. In equations 7 and 8, \hat{I} represents the coarsely adjusted image in the first stage and the final output

image in the second stage, respectively. It should be noted that in L_{refine} , we only focus on the submask area, so the loss is multiplied by the submask. Furthermore, We find that the images with small foreground masks are always hard examples and we want our model to learn more information from them. Therefore, we divide the loss by the area of the foreground mask. A_{min} is a constant, which is set to 100 in all the experiments. For those foreground masks whose areas are smaller than A_{min} , we treat them as A_{min} .

4 EXPERIMENTS

4.1 Datasets and Evaluation Metrics

To demonstrate the effectiveness of our FRIH, we conduct experiments on the public image harmonization dataset iHarmony4 [8]. This dataset consists of four sub-datasets, including HCOCO,

Table 3: Ablation study in each sub-dataset on iHarmony4 test set.

Sub-dataset Metric	HCOCO		HADobe5k		HFlickr		Hday2night		All	
	MSE↓	PSNR↑								
Input composite	69.37	33.94	345.54	28.16	264.35	28.32	109.65	34.01	172.47	31.63
Baseline	21.38	38.24	37.15	35.79	90.12	32.25	50.12	37.45	35.38	36.82
Baseline+Cascade	16.52	39.09	26.21	37.42	75.82	33.05	44.21	37.78	26.31	37.90
Baseline+Cascade+Fusion	15.05	39.35	23.61	37.69	68.93	33.48	42.78	37.89	23.98	38.19

Table 4: Ablation study in each foreground ratio range on iHarmony4 test set.

Foreground ratios Metric	0%-5%		5%-15%		15%-100%		All	
	MSE↓	fMSE↓	MSE↓	fMSE↓	MSE↓	fMSE↓	MSE↓	fMSE↓
Input composite	28.51	1208.86	119.19	1323.23	577.58	1887.05	172.47	1387.30
Baseline	10.21	421.53	29.68	336.32	109.21	345.19	35.38	380.12
Baseline+Cascade	7.28	322.86	21.42	244.15	77.82	230.47	26.31	268.52
Baseline+Cascade+Fusion	6.89	305.28	19.88	226.45	70.05	205.83	23.98	252.63

HADobe5k, HFlickr and Hday2night. There are totally 65,742 training image pairs and 7,407 test image pairs in iHarmony4. All the image pairs are generated by modifying the specific foreground regions of the normal images, which are converted to corresponding the inharmonic images in this way. We follow the same train-test split as DoveNet [8] in the experiments.

Following prior work [8, 33], we use Mean Squared Error (MSE) scores and Peak Signal-to-Noise Ratio (PSNR) scores on RGB channels to evaluate the image harmonization performance. Besides, to eliminate the influence of the foreground area size on the metric, we also introduced the foreground Mean Squared Error (fMSE) score [8]. Note that all the input and output images are resized to 256×256 resolution during training and test, thus all the evaluation metrics are calculated based on the 256×256 resolution.

4.2 Implementation details

We use Adam Optimizer with $\beta_1 = 0.9$ and $\beta_2 = 0.999$ to train our model for 180 epochs on 8 Tesla V100 GPUs. The initial learning rate is 0.008, which decays by 10 at epoch 160 and 175. The batchsize is 128. All the images are resized to 256×256 in both training and test process. We use horizontal flip and random size crop to augment the data during training. The whole FRIH network is trained end-to-end. The cutoff distance d_c is set to 0.1.

4.3 Comparison with the State-of-the-Art

We compare our FRIH with other image harmonization methods on iHarmony4. Table 1 and Table 2 separately show the results in each sub-dataset and each foreground ratio range. From Table 1 and Table 2 we can find that:

(1) Our method achieves 38.19 PSNR and 23.98 MSE on iHarmony4 test set, which performs better than all the other image harmonization methods on iHarmony4 test set in a large margin. Compared to the previous SOTA methods, the PSNR of our method

has an obvious improvement. The latest transformer-based method D-HT [13] achieved 37.55 using a large model. While our method is the only one whose PSNR is larger than 38 dB, which proves that the fine-grained region-aware framework works well. It should be noted that iDIH [29] obtains higher performance than 37.08 dB when adding extra pre-trained semantic segmentation model, which all other methods do not use. It is unfair to make comparison so that we only show their results without the extra model.

(2) In Table 1, our method performs much better than existing methods on all of the 4 sub-datasets, demonstrating the robustness of our cascaded module and fusion prediction strategy.

(3) In Table 2, our method performs better than all the existing methods on the composite images with different foreground ratio, proving that our submask extraction is well adaptive regardless of the foreground area size.

4.4 Ablation Study

We compare the following models on iHarmony4 dataset to show the effectiveness of FRIH's parts:

- *Input composite*. It means that we directly use the input composite image as the final output result, without any harmonization processing.
- *Baseline*. The baseline only uses the base network to make a coarse-grained harmonization, without the submask extraction and the lightweight cascaded module.
- *Baseline+Cascade*. We extract submasks adaptively for each foreground mask and feed the concatenation of each submask and the coarsely adjusted image into the lightweight cascaded module.
- *Baseline+Cascade+Fusion (FRIH)*. This is the full version of our algorithm, including the submask extraction, lightweight

Table 5: Comparative experiment in terms of d_c on iHarmony4 test set.

d_c	0.01	0.05	0.1	0.2	0.3	0.4
MSE↓	25.26	24.49	23.98	24.76	25.41	25.90
PSNR↑	38.09	38.17	38.19	38.15	38.08	38.02

cascaded module together with the fusion prediction strategy. We use features from all the cascaded decoder layers to predict the final harmonized results.

The ablation study results in each sub-dataset and each foreground ratio range on iHarmony4 are presented in Table 3 and Table 4 respectively, showing that:

(1) Both the lightweight cascaded module and fusion prediction strategy can increase PSNR and decrease MSE. *Baseline+Cascade* performs significantly better *Baseline* with the gain of 1.08 dB in PSNR. *Baseline+Cascade+Fusion* outperforms *Baseline+Cascade* with the gain of 0.29 dB in PSNR. It demonstrates the effectiveness of both the lightweight cascaded module and the fusion prediction strategy. Compared to *Baseline*, our FRIH has a gain of 1.37 dB in PSNR and a decrease of 11.40 in MSE metric, proving that the whole global-local framework is effective and all modules are reciprocal.

(2) The effectiveness of the lightweight cascaded module is not very apparent on Hday2night sub-dataset. We analyze the composite images and the foreground masks. We find that the foreground areas in Hday2night are always sky, water surface or other similar categories with single and pure color. These areas are homogeneous. Therefore, it is hard to separate these foreground areas into different sub-regions, making our cascaded module useless. From another perspective, it further proves the effectiveness of our method on foregrounds with different appearance patterns. By the way, our fusion prediction strategy still works on Hday2night, since it is not affected by submasks.

(3) The increase of PSNR between *Baseline* and *Baseline+Cascade* on HAobe5k sub-dataset achieves 1.63, which is the largest among 4 sub-datasets in Table 3. We think the reason is that the foreground masks in HAobe5k are much bigger than other three sub-datasets, which means these bigger foreground masks are more likely to contain disparate sub-regions or different appearance patterns. The baseline model treats them in the same way while the cascaded module can adjust them adaptively, leading to a significantly increase of PSNR and decrease of MSE.

(4) The increase between *Baseline* and *Baseline+Cascade* of images whose foreground mask sizes are larger than 15% is also the biggest in Table 4. We believe the reason is as same as the reason why the increase in the sub-dataset HAobe5k is the biggest. Both (3) and (4) can prove that our submasks-based cascaded module is efficient for image harmonization task, especially for those images with large foreground masks.

Moreover, the cutoff distance d_c in the submask extraction module is a significant hyper-parameter in our method. It determines the granularity of the submasks division. We conduct comparative experiment in terms of d_c on iHarmony4 test set. The results are shown in Table 5. d_c is set to 0.01, 0.05, 0.1, 0.2, 0.3 and 0.4, respectively. When $d_c = 0.1$, our FRIH achieves the best performance.

Table 6: Comparison of Model Size and GFLOPS.

Method	Params↓	GFLOPS↓	PSNR↑
DoveNet [8]	54.76	18.97	34.75
IIH [14]	40.83	196.3	35.90
RainNet [19]	54.75	18.95	36.12
FRIH (ours)	11.98	25.12	38.19

Table 7: Comparison between our FRIH and other state-of-the-art methods under user study.

Method	Input	DoveNet	RainNet	FRIH (Ours)
Votes↑	261	485	501	733
Preference↑	12.1%	23.2%	24.1%	40.6%

Thus we set $d_c = 0.1$ in all the other experiments in this paper. When $d_c = 0.01$, the performance is lower than $d_c = 0.1$, because the clustering is so fine-grained that many noisy isolated outliers are generated and have negative effect on the selection of cluster centers. When $d_c = 0.3$ and $d_c = 0.4$, the performance also drops compared with $d_c = 0.1$, which is caused by the too coarse-grained clustering. Several color blocks, which are not similar, are clustered into a same cluster. However, The PSNR in all these experiments exceeds 38, demonstrating the robustness of our method.

4.5 Comparison of Model Size and Computation

We also compare the model size and computation of our method FRIH with existing SOTA methods. As shown in Table 6, compared to existing methods, our FRIH method achieves much higher results while the model size is only about 1/5 of theirs. The computation cost of our model is also close to the computation of DoveNet [8] and RainNet [19], and much lower than that of IIH [14].

4.6 User Study

Sometimes the PSNR and MSE metrics can not correctly reflect the impressions of human eyes. Thus, we conduct the user study on 99 images dataset provided by DIH [33]. We invite 20 volunteers and ask them to select the most realistic images they think from composite images and results generated by DoveNet [8], RainNet [19] and our FRIH. The total number of votes are 1980. As shown in Table 7, our FRIH attains much more votes than other state-of-the-art methods, which proves that our method not only performs best on PSNR and MSE metrics, but also can generate more realistic images than other methods according to human judgement.

4.7 Qualitative Analysis

We show some visualization results on iHarmony4 test dataset of our FRIH method against DoveNet [8] and RainNet [19] in Figure 5. In all the 5 cases, the harmonization images of our FRIH are more

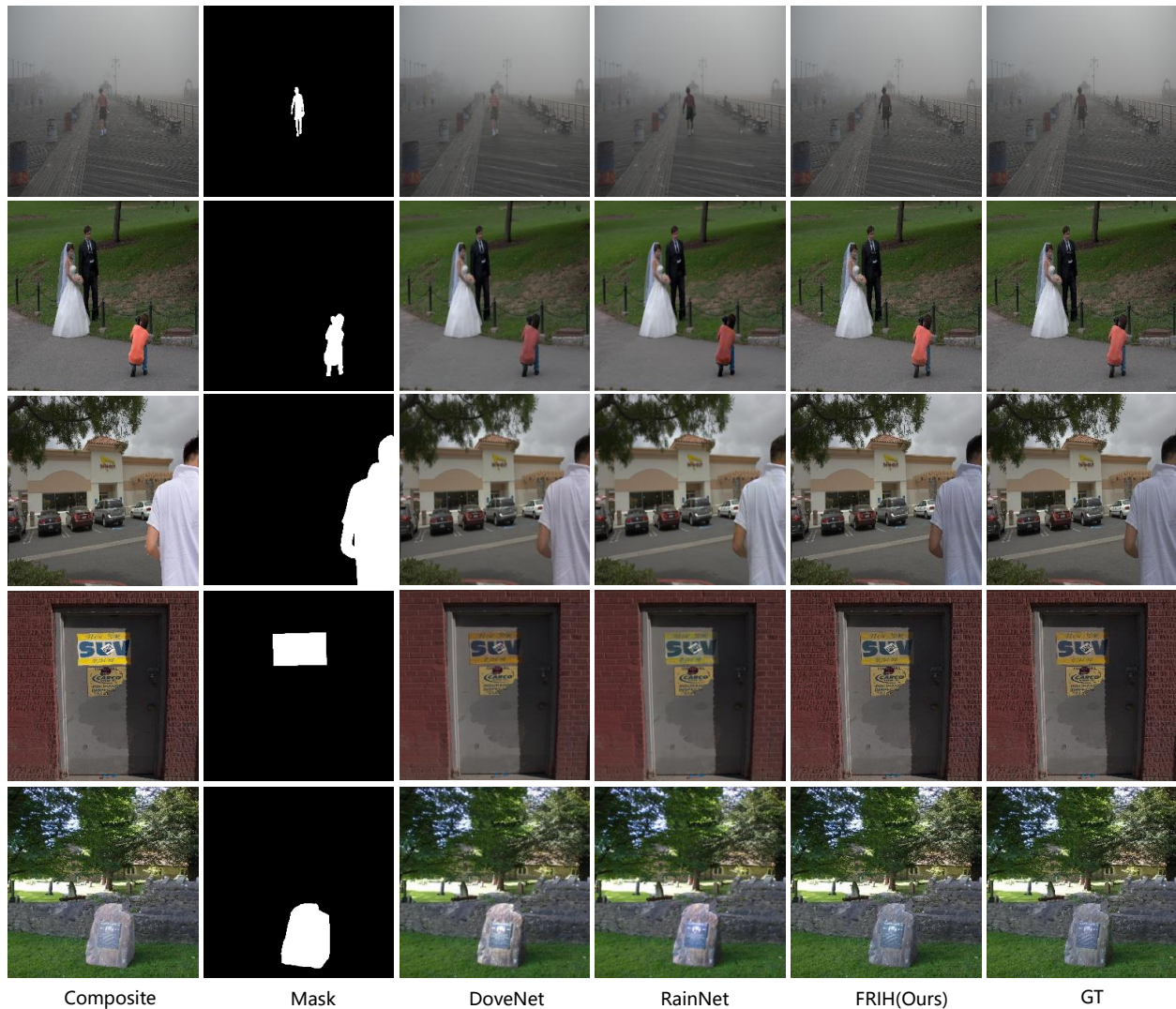


Figure 5: Qualitative comparison between our FRIH and other state-of-the-art methods.

closer to the ground-truth images compared to DoveNet [8] and RainNet [19]. The foreground in each case has different appearance patterns. Applying DoveNet and RainNet, only part of the foreground has satisfactory harmonization performance. For example, in the fourth line, the blue word 'SUV' is handled well while the yellow poster is not, both in DoveNet and RainNet. However, our FRIH algorithm handles the details of all the sub-regions better, demonstrating the effectiveness of our fine-grained region-aware framework. Some representative visualization results of our FRIH method against DoveNet [8] and RainNet [19] on the 99 image test dataset [33] are presented in the supplementary materials.

5 CONCLUSION

We proposed a two-stage fine-grained region-aware image harmonization framework, which is simple, novel and effective. In the first stage, the whole input foreground mask is used to make a global

coarse-grained harmonization. In the second stage, we adaptively cluster the input foreground mask into several submasks by the corresponding pixel RGB values. Each submask and the coarsely adjusted image are concatenated respectively and fed into the lightweight cascaded module. Moreover, we further designed a fusion prediction module by fusing features from all the cascaded decoder layers together to generate the final result. It addresses the problem that existing methods ignore the difference of each color block and loses some specific details. Extensive experimental results demonstrate the effectiveness and efficiency of our FRIH algorithm and its superiority over the state-of-the-art competitors on iHarmony4.

REFERENCES

- [1] Samaneh Azadi, Deepak Pathak, Sayna Ebrahimi, and Trevor Darrell. 2020. Compositional gan: Learning image-conditional binary composition. *International Journal of Computer Vision* 128, 10 (2020), 2570–2585.

- [2] Zhaowei Cai and Nuno Vasconcelos. 2018. Cascade r-cnn: Delving into high quality object detection. In *Proceedings of the IEEE conference on computer vision and pattern recognition*. 6154–6162.
- [3] Bor-Chun Chen and Andrew Kae. 2019. Toward realistic image compositing with adversarial learning. In *Proceedings of the IEEE/CVF Conference on Computer Vision and Pattern Recognition*. 8415–8424.
- [4] Kai Chen, Jiangmiao Pang, Jiaqi Wang, Yu Xiong, Xiaoxiao Li, Shuyang Sun, Wansen Feng, Ziwei Liu, Jianping Shi, Wanli Ouyang, et al. 2019. Hybrid task cascade for instance segmentation. In *Proceedings of the IEEE/CVF Conference on Computer Vision and Pattern Recognition*. 4974–4983.
- [5] Yu Cheng, Zhe Gan, Yitong Li, Jingjing Liu, and Jianfeng Gao. 2020. Sequential attention GAN for interactive image editing. In *Proceedings of the 28th ACM International Conference on Multimedia*. 4383–4391.
- [6] Daniel Cohen-Or, Olga Sorkine, Ran Gal, Tommer Leyvand, and Ying-Qing Xu. 2006. Color harmonization. In *Proceedings of SIGGRAPH*.
- [7] Wenyang Cong, Li Niu, Jianfu Zhang, Jing Liang, and Liqing Zhang. 2021. Bargainnet: Background-Guided Domain Translation for Image Harmonization. In *IEEE International Conference on Multimedia and Expo*.
- [8] Wenyang Cong, Jianfu Zhang, Li Niu, Liu Liu, Zhixin Ling, Weiyan Li, and Liqing Zhang. 2020. Dovenet: Deep image harmonization via domain verification. In *Proceedings of the IEEE conference on computer vision and pattern recognition*.
- [9] Xiaodong Cun and Chi-Man Pun. 2020. Improving the harmony of the composite image by spatial-separated attention module. *IEEE Transactions on Image Processing* (2020).
- [10] Alexey Dosovitskiy, Lucas Beyer, Alexander Kolesnikov, Dirk Weissenborn, Xiuhua Zhai, Thomas Unterthiner, Mostafa Dehghani, Matthias Minderer, Georg Heigold, Sylvain Gelly, et al. 2021. An image is worth 16x16 words: Transformers for image recognition at scale. (2021).
- [11] Karol Gregor, Ivo Danihelka, Alex Graves, Danilo Rezende, and Daan Wierstra. 2015. Draw: A recurrent neural network for image generation. In *International Conference on Machine Learning*. PMLR, 1462–1471.
- [12] Zongyu Guo, Zhibo Chen, Tao Yu, Jiale Chen, and Sen Liu. 2019. Progressive image inpainting with full-resolution residual network. In *Proceedings of the 27th acm international conference on multimedia*. 2496–2504.
- [13] Zonghui Guo, Dongsheng Guo, Haiyong Zheng, Zhaorui Gu, Bing Zheng, and Junyu Dong. 2021. Image Harmonization With Transformer. In *Proceedings of the IEEE/CVF International Conference on Computer Vision*. 14870–14879.
- [14] Zonghui Guo, Haiyong Zheng, Yufeng Jiang, Zhaorui Gu, and Bing Zheng. 2021. Intrinsic Image Harmonization. In *Proceedings of the IEEE conference on computer vision and pattern recognition*.
- [15] Guoqing Hao et al. 2020. Image Harmonization with Attention-based Deep Feature Modulation. In *The British Machine Vision Conference*.
- [16] Jiaya Jia, Jian Sun, Chi-Keung Tang, and Heung-Yeung Shum. 2006. Drag-and-drop pasting. *ACM Transactions on graphics* (2006).
- [17] Yifan Jiang, He Zhang, Jianming Zhang, Yilin Wang, Zhe Lin, Kalyan Sunkavalli, Simon Chen, Sohrab Amirghodsi, Sarah Kong, and Zhangyang Wang. 2021. SSH: A Self-Supervised Framework for Image Harmonization. In *Proceedings of the IEEE/CVF International Conference on Computer Vision*. 4832–4841.
- [18] Jean-Francois Lalonde and Alexei A Efros. 2007. Using color compatibility for assessing image realism. In *IEEE/CVF International Conference on Computer Vision*.
- [19] Jun Ling, Han Xue, Li Song, Rong Xie, and Xiao Gu. 2021. Region-aware Adaptive Instance Normalization for Image Harmonization. In *Proceedings of the IEEE conference on computer vision and pattern recognition*.
- [20] Dong Liu, Rohit Puri, Nagendra Kamath, and Subhabrata Bhattacharya. 2020. Composition-aware image aesthetics assessment. In *Proceedings of the IEEE/CVF Winter Conference on Applications of Computer Vision*. 3569–3578.
- [21] Hongying Liu, Xiongjie Shen, Fanhua Shang, Feihang Ge, and Fei Wang. 2019. CU-Net: Cascaded U-Net with loss weighted sampling for brain tumor segmentation. In *Multimodal Brain Image Analysis and Mathematical Foundations of Computational Anatomy*. Springer, 102–111.
- [22] Jinlong Peng, Changan Wang, Fangbin Wan, Yang Wu, Yabiao Wang, Ying Tai, Chengjie Wang, Jilin Li, Feiyue Huang, and Yanwei Fu. 2020. Chained-tracker: Chaining paired attentive regression results for end-to-end joint multiple-object detection and tracking. In *European Conference on Computer Vision*. Springer, 145–161.
- [23] Patrick Pérez, Michel Gangnet, and Andrew Blake. 2003. Poisson image editing. In *Proceedings of SIGGRAPH*.
- [24] François Pitié and Anil Kokaram. 2007. The linear monge-kantorovitch linear colour mapping for example-based colour transfer. In *European Conference on Computer Vision*.
- [25] Francois Pitié, Anil C Kokaram, and Rozenn Dahyot. 2005. N-dimensional probability density function transfer and its application to color transfer. In *IEEE/CVF International Conference on Computer Vision*.
- [26] Haonan Qiu, Chaowei Xiao, Lei Yang, Xinchun Yan, Honglak Lee, and Bo Li. 2020. SemanticAdv: Generating Adversarial Examples via Attribute-conditioned Image Editing. In *European Conference on Computer Vision*. Springer, 19–37.
- [27] Alex Rodriguez and Alessandro Laio. 2014. Clustering by fast search and find of density peaks. *science* 344, 6191 (2014), 1492–1496.
- [28] Olaf Ronneberger, Philipp Fischer, and Thomas Brox. 2015. U-net: Convolutional networks for biomedical image segmentation. In *International Conference on Medical Image Computing and Computer Assisted Intervention*.
- [29] Konstantin Sofiiuk, Polina Popenova, and Anton Konushin. 2021. Foreground-aware Semantic Representations for Image Harmonization. In *Proceedings of the IEEE/CVF Winter Conference on Applications of Computer Vision*. 1620–1629.
- [30] Shuangbing Song, Fan Zhong, Xueying Qin, and Changhe Tu. 2020. Illumination harmonization with gray mean scale. In *Computer Graphics International Conference*. Springer, 193–205.
- [31] Kalyan Sunkavalli, Micah K Johnson, Wojciech Matusik, and Hanspeter Pfister. 2010. Multi-scale image harmonization. *ACM Transactions on Graphics* (2010).
- [32] Michael W Tao, Micah K Johnson, and Sylvain Paris. 2013. Error-tolerant image compositing. *International journal of computer vision* (2013).
- [33] Yi-Hsuan Tsai, Xiaohui Shen, Zhe Lin, Kalyan Sunkavalli, Xin Lu, and Ming-Hsuan Yang. 2017. Deep image harmonization. In *Proceedings of the IEEE conference on computer vision and pattern recognition*.
- [34] Aaron Van den Oord, Nal Kalchbrenner, Lasse Espeholt, Oriol Vinyals, Alex Graves, et al. 2016. Conditional image generation with pixelcnn decoders. *Advances in neural information processing systems* 29 (2016).
- [35] Ashish Vaswani, Noam Shazeer, Niki Parmar, Jakob Uszkoreit, Llion Jones, Aidan N Gomez, Łukasz Kaiser, and Illia Polosukhin. 2017. Attention is all you need. *Advances in neural information processing systems* 30 (2017).
- [36] Jin Wang, Chen Wang, Qingming Huang, Yunhui Shi, Jian-Feng Cai, Qing Zhu, and Baocai Yin. 2020. Image inpainting based on multi-frequency probabilistic inference model. In *Proceedings of the 28th ACM International Conference on Multimedia*. 1–9.
- [37] Rongliang Wu, Gongjie Zhang, Shijian Lu, and Tao Chen. 2020. Cascade ef-gan: Progressive facial expression editing with local focuses. In *Proceedings of the IEEE/CVF Conference on Computer Vision and Pattern Recognition*. 5021–5030.
- [38] Su Xue, Aseem Agarwala, Julie Dorsey, and Holly Rushmeier. 2012. Understanding and improving the realism of image composites. *ACM Transactions on graphics* (2012).
- [39] Fangneng Zhan, Shijian Lu, Changgong Zhang, Feiying Ma, and Xuansong Xie. 2020. Adversarial image composition with auxiliary illumination. In *Proceedings of the Asian Conference on Computer Vision*.
- [40] Jun-Yan Zhu, Philipp Krahenbuhl, Eli Shechtman, and Alexei A Efros. 2015. Learning a discriminative model for the perception of realism in composite images. In *IEEE/CVF International Conference on Computer Vision*.